ORIGINAL ARTICLE

Continuous Models for Cell Migration in Tissues and Applications to Cell Sorting via Differential Chemotaxis

Kevin J. Painter

Department of Mathematics and Maxwell Institute for Mathematical Sciences, School of Mathematical and Computer Sciences, Heriot-Watt University, Edinburgh EH14 4AS, UK

Abstract Chemotaxis, the guided migration of cells in response to chemical gradients, is vital to a wide variety of biological processes, including patterning of the slime mold *Dictyostelium*, embryonic morphogenesis, wound healing, and tumor invasion. Continuous models of chemotaxis have been developed to describe many such systems, yet few have considered the movements within a heterogeneous tissue composed of multiple subpopulations. In this paper, a partial differential equation (PDE) model is developed to describe a tissue formed from two distinct chemotactic populations. For a "crowded" (negligible extracellular space) tissue, it is demonstrated that the model reduces to a simpler one-species system while for an "uncrowded" tissue, it captures both movement of the entire tissue (via cells attaching to/migrating within an extracellular substrate) and the within-tissue rearrangements of the separate cellular subpopulations. The model is applied to explore the sorting of a heterogeneous tissue, where it is shown that differential-chemotaxis not only generates classical sorting patterns previously seen via differential-adhesion, but also demonstrates new classes of behavior. These new phenomena include temporal dynamics consisting of a traveling wave composed of spatially sorted subpopulations reminiscent of *Dictyostelium* slugs.

1. Introduction

Morphogenesis, the patterning of a developing embryo, is contingent on the complex interplay of a multitude of intracellular and intercellular signaling pathways, leading to the precise spatio-temporal triggering of cell behavior, including division, apoptosis, differentiation, and cell movement. Various theoretical models have been proposed to explain morphogenetic patterning. In chemical prepattern models such as the Turing reaction–diffusion model (Turing, 1952), graded chemical signals provide the "positional information" (Wolpert, 1969) to differentiate cells while in mechanochemical (e.g., Murray, 2003)

E-mail address: K.J.Painter@ma.hw.ac.uk.

or chemotaxis models (e.g., Hillen and Painter, 2009), it is the dynamical interaction between the cells and their surrounding environment (e.g., extracellular matrix (ECM), chemoattractants) that drives spatial pattern formation.

Cell movement plays numerous roles during both embryonic patterning and functioning of the adult organism. Migration can occur either as the coordinated movement of entire cell tissues, sheets, and clusters (collective cell migration) or through the movement of cells as individual objects (individual cell migration), for a review, see Friedl and Brocker (2000). The environment in which cells migrate also varies. Certain cells, such as fibroblasts and leukocytes, have the capacity to move within sparsely populated (i.e., low cell density) environments such as the dermal layer of the skin. In many cases, however, migration can continue even within a densely populated (high cell density) environment with limited extracellular space, for example, the migration of border cell clusters in *Drosophila* (Montell, 2006), the rearrangement of epithelial monolayers during insect wing development (Nardi, 1994), the infiltration of solid tumors by macrophages (Murdoch et al., 2004), and the movement of individual cells within slime mold aggregation mounds (Early et al., 1995). For dense tissues, an important question arises concerning how movement of one cell population impacts on the distribution of another population.

The movement of eukaryotic cells such as fibroblasts or *Dictyostelium* is a multistep process involving the extension of cell protrusions (e.g., lamellipodia, pseudopodia, filopodia), attachment to an external substrate through the formation of adhesion complexes, translocation of the cell body, and detachment at the rear of the cell (Lauffenburger and Horwitz, 1996). Creation of the adhesion complexes is vital: They provide anchoring points for transmitting the forces required for movement as well as stimulating biochemical signaling processes. For movement in sparsely populated structures, such as the dermis, these anchor the cell to the surrounding extracellular matrix. In a dense cellular tissue, the cells form their adhesion complexes with neighboring cells and the forces generated by a moving cell are therefore exerted on its neighbors. Effectively, a cell can pull itself forward only by pulling other cells back and the net local movement will therefore be zero (see also Odell and Bonner, 1986; Dallon and Othmer, 2004): for *tissue-level* movement to occur their must be an attachment to some surrounding rigid structure.

Coordinated migration hinges on the ability of cells to translate and integrate external guidance cues into a specific movement response. Cues include oxygen or extracellular chemicals (e.g., chemoattractants and repellents), the ECM (e.g., haptotaxis, contact guidance) and interactions with other cells (e.g., cell-cell adhesion or contact guidance). Chemotaxis, the guidance of cells in response to chemical gradients, is essential to many biological cell populations. For bacteria, chemotaxis guides cells to nutrients and away from harmful substances. During development, chemotaxis has been identified in a number of processes: in the chick embryo, primitive streak cells navigate via a combination of attractive and repulsive responses to members of the FGF family (Yang et al., 2002; Dormann and Weijer, 2006); a repulsive response to Wnt-3a directs cardiac progenitors during early heart formation (Yue et al., 2008); patterning of the nervous system is coordinated through growth cone guidance to a multitude of attractive and repulsive chemotactic factors (Charron and Tessier-Lavigne, 2005). Chemotaxis continues to operate in the adult, notably in the responses of fibroblasts to PDGF during wound healing (Heldin and Westermark., 1999) or as part of the immune response to infection (Wu, 2005). Chemotaxis occurs at various stages of tumor development, including angiogenesis (Larrivee
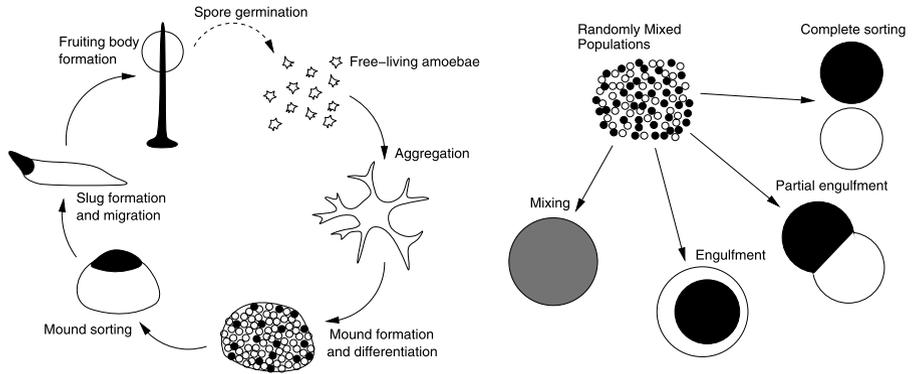
Fig. 1 Left: schematic of stages in the *Dictyostelium* lifecycle. Right: cell sorting for two adhesive populations u (black) and v (white): following disassociation and random mixing of the cell types, "sorting" occurs in which the cell populations reassemble into distinct spatial configurations. According to the *Differential-adhesion hypothesis*, these configurations depend on the self-adhesion S_u, S_v (between u and u, between v and v) and cross-adhesion C (between u and v) strengths. For two populations, the observed patterns are *mixing* (in which the populations are uniformly distributed—requires dominant cross adhesion $C > \frac{S_u + S_v}{2}$), *engulfment* (in which the more cohesive population is engulfed by the less cohesive population—requires $S_v < C < S_u$ (or $S_u < C < S_v$)), *partial engulfment* (for which the cross adhesion strength is less than both the self adhesion strengths—$C < S_u$ and $C < S_v$) and *complete sorting* (for which $C = 0$ and the two populations form separate aggregations). Figure adapted from Foty and Steinberg (2004).

and Karsan, 2000), cancer invasion (Condeelis et al., 2005) and macrophage infiltration of tumors (Murdoch et al., 2004).

A classic *in vivo* example of chemotactic-driven patterning lies at the heart of morphogenesis in the cellular slime mold *Dictyostelium discoideum* (Fig. 1; see also the reviews in Dormann and Weijer, 2006; Kimmel and Firtel, 2004). In an abundant nutrient environment, *Dictyostelium* cells exist as dispersed and free-living single amoebae. Starvation induces their organization into dense multicellular aggregates (mounds) composed of approximately 100,000 cells. Differentiation generates distinct subpopulations of prespore and prestalk cell types which are initially dispersed throughout the mound, but subsequently undergo "spatial sorting" resulting in the compartmentalization of prestalk cells to the mound top. The mound transforms into a migrating "slug" which undergoes further differentiation and pattern formation, finally evolving into a fruiting body composed of dead and vacuolated stalk cells which support the surviving spores until more favorable environmental conditions allow their germination and rerelease as single amoebae. Both during the initial aggregation of the single amoebae and the subsequent reorganization of the cells within mounds and slugs, cells remain highly mobile and their movement is coordinated via a chemotactic relaying system in which the amoebae migrate up gradients of the chemical cAMP, produced by the cells themselves.

The ability of cells to spatially sort within a dense/cellular tissue is also crucial to embryonic development, the organs of which form with the distinct tissue layers (epidermis, mesoderm, endoderm) precisely arranged. Classic experiments by Townes and Holtfreter (1955) demonstrated that following the disassociation and random mixing of distinct embryonic populations they were able to reorganize back into their original embryonic arrangement. A long series of theoretical and experimental studies by Steinberg

et al. (see Foty and Steinberg, 2004; Steinberg, 2007 for reviews) led to the "differential-adhesion hypothesis": differences in the numbers and types of cell adhesion molecules at the cell membrane would result in local cell rearrangements, eventually leading to macroscopic organization. The final configuration of the populations would be determined by the self-adhesion (between two cells of the same type) and cross-adhesion (between two cells of different type) strengths; see Fig. 1. Theoretical investigations using both discrete (e.g., Glazier and Graner, 1993; Palsson and Othmer, 2000) and continuous (e.g., Armstrong et al., 2006) models have demonstrated the capacity for differential adhesion to pattern a heterogeneous tissue.

Clearly, sorting can be driven solely through the local rearrangement of cells via differential-adhesion. As described above, in many morphogenetic processes longer range signaling cues such as chemoattractants play a role—for *Dictyostelium* the chemical cAMP serves as a chemotactic cue while in chick gastrulation primitive streak cells are attracted by gradients of FGF-4 and repelled by gradients of FGF-8. These examples raise the question as to whether differential responses to long range signals such as chemoattractants can pattern/organize a heterogeneous tissue. However, despite the numerous theoretical investigations exploring differential-adhesion induced patterning, a corresponding study into differential-chemotaxis is lacking. In the context of *Dictyostelium* slug patterning, it is known that prespore and prestalk cells have distinct motility responses (Early et al., 1995) and differential chemotaxis has been postulated as a mechanism for driving this sorting (Matsukuma and Durston, 1979). A variety of theoretical models have shown that differential chemotaxis may pattern the *Dictyostelium* slug (e.g., Pate and Othmer, 1986; Vasiev and Weijer, 1999; Palsson and Othmer, 2000; Umeda and Inouye, 2004).

1.1. Paper outline

The aim is to derive continuous equations capable of describing a heterogeneous tissue composed of multiple motile cell subpopulations. Specifically, the model will be judged on its capacity to allow both tissue-level movement *and* within-tissue movements of the separate subpopulations. In the next section, the relevant modeling is reviewed and its limitations (with respect to the above objectives) highlighted. In Section 3, a phenomenological approach is employed to motivate the derivation of a continuous PDE model, while in Section 4, its suitability is explored. In Section 5, the model is applied to explore the capacity for differential chemotaxis to drive sorting/patterning of a heterogeneous tissue. The paper concludes with a discussion of the results and an outlook to future explorations.

2. Modeling cell movement in tissues

Various methods are employed to model population-level chemotactic movement. Broadly, these can be classified as either discrete or continuous: In the former, cells are modeled as discrete objects, while in the latter populations are represented by continuous variables for the cell densities. Discrete models offer certain advantages, such as the ease by which cell interactions or extra populations can be incorporated, yet their numerically taxing character and the difficulty of extracting analytical insight encourages simultaneous development and study of continuous models.

2.1. *Continuous models for chemotaxis: single cell population models*

Continuous modeling of chemotaxis dates to the seminal works of Patlak in the 1950s (Patlak, 1953) and Keller and Segel in the 1970s (Keller and Segel, 1970, 1971). The Keller–Segel model, initially developed to describe aggregation of *Dictyostelium*, forms a cornerstone for modeling chemotaxis. In its basic form, this system comprises a pair of coupled partial differential equations for the cell density $u(x, t)$ and chemical concentration $a(x, t)$:

$$u_t = \nabla\big(D_u(u, a)\nabla u - \chi(u, a)u\nabla a\big) + f(u, a), \tag{1a}$$

$$a_t = D_a\nabla^2 a + g(u, a). \tag{1b}$$

In the above, cell dynamics derive from population kinetics and movement, the latter comprising a diffusive flux modeling undirected (random) cell migration and an advective flux with velocity dependent on the gradient of the signal, modeling the contribution of chemotaxis. $D_u(u, a)$ describes the diffusivity of the cells while $\chi(u, a)$ is the chemotactic sensitivity: generally, both functions will depend on both the levels of u and a. f and g, respectively, describe cell growth and signal kinetics. Often, cells migrate in response to externally generated chemical gradients, e.g., the response of commisural axons to gradients of various factors secreted at the floor plate (Charron and Tessier-Lavigne, 2005), and the impact of cells on the chemical distribution may be relatively small. In other instances, the cells may play a major role in the signal dynamics either through producing it or regulating its degradation, an apt example being the regulation of cAMP by *Dictyostelium* cells. The incorporation of cell-regulated chemical dynamics into Eqs. (1) has received significant attention due to its capacity to generate *self-organization*: an autocrine-type mechanism in which cells migrate up gradients of a self-secreted signal can result in their accumulation into aggregation mounds. This spatial patterning property of the Keller–Segel equations has contributed to their extension to a variety of models for biological patterning, including stages in the lifecycle of *Dd* (e.g., Keller and Segel, 1970; Höfer et al., 1995) or pattern formation in bacteria (e.g., Woodward et al., 1995; Tyson et al., 1999).

Under certain formulations of Eqs. (1) this self aggregating property has been shown to lead to finite time "blow-up" in which cell densities form singularities. Evolution to infinite cell densities, however, is biologically/physically unrealistic and reveals limitations in the specific formulation of the model. A focus for a number of studies has been to derive (biologically) plausible and "regularized" forms of Eqs. (1) for which solutions do not blow-up: the review by Hillen and Painter (2009) describes a number of these models in detail.

One such method was to incorporate the effects of a maximum tissue density (Hillen and Painter, 2001; Painter and Hillen, 2002): the singularity formation observed in the minimal model generates infinite cell densities, thereby neglecting the finite-size of biological cells. Via the assumption that movement occurs only if there is sufficient available space, a class of *volume-filling* models is derived that incorporates a cell density-dependent chemotactic sensitivity. In its simplest form,

$$u_t = D_u\nabla^2 u - \chi_u\nabla\big(u(1 - u/k)\nabla a\big), \tag{2a}$$

$$a_t = D_a\nabla^2 a + \gamma u - \delta a \tag{2b}$$

with initial data $0 \leq u(x, 0) \leq k$ (where k represents the "maximum tissue density"). For appropriate parameter values, the above permits aggregations to develop yet solutions do not blow-up and remain bounded below the maximum tissue density.

2.2. Continuous models for chemotaxis: multiple population models

Many biological tissues are heterogeneous and can contain multiple populations with distinct motility properties, e.g., the subpopulations generated during *Dictyostelium* morphogenesis or the guidance of cells into distinct tissue layers during embryonic gastrulation. For a cell to move within a tissue, it must form adhesion complexes with either the surrounding ECM/extracellular surface, other cells (in packed tissues) or a combination; clearly at high cell densities the movement of one population may significantly impact on the movement of another. While the incorporation of additional populations into discrete chemotaxis models is relatively straightforward, their incorporation into continuous models poses a number of challenges.

Trivially, the equation for u in (1) can be replaced with a set of equations representing the evolution of the densities for the various cell populations. The question arises as to how the movement of one population is influenced by the other cells, i.e., the appropriate dependence of the functions D_u and χ on the population densities. For highly dispersed populations or low density tissues, it may be reasonable to assume movement is independent of other cells (e.g., Sherratt and Nowak, 1992). For denser tissues, however, cell contacts are inevitable and the impact of cell interactions should be considered. Despite this, relatively few continuous models have investigated this aspect.

One method is to adopt phenomenological reasoning. For example, Gatenby and Gawlinski (1996) develop a reaction–diffusion model describing tumor invasion into healthy tissue in which tumor cell invasion was represented by a diffusion coefficient decreasing with increasing healthy tissue density, i.e., a denser tissue was assumed to reduce the capacity for the tumor cells to invade. More sophisticated derivations were attempted by Sherratt (2000) to model "contact-inhibition" between two cell types and Painter and Sherratt (2003) through a discrete lattice approach; in the PDE models that followed the movements of one population intrinsically depended on the distributions of other populations. Simpson et al. (2006) have used similar continuous models to model the invasion of a population of grafted neural crest cells into a host tissue. In the applications of these models, it was demonstrated that increasing tissue densities could significantly impede movement, even culminating in the "trapping" of a population at packed densities. This model response may be reasonable to describe certain cell types (e.g., contact-inhibited populations or flagellar bacteria such as *E. coli*), yet is clearly inadequate as a description for the continued movement of other cell types in dense tissues, for example, the prestalk and prespore cells within the *Dictyostelium* mound as described earlier.

An alternative approach to model movement of multiple subpopulations in a tissue is to employ mass-conservation and multiphase methods. Pate and Othmer (1986) considered the former for the patterning of prespore/prestalk cells within *Dictyostelium* by representing the slug as a heterogeneous tissue at a constant total cell density. Subpopulations inside the slug were assumed to move by displacing others such that the total density is preserved; a number of expansions have been considered (e.g., Umeda, 1993; Umeda and Inouye, 1999). Significantly, these authors demonstrated that differences in the chemotactic responses of the subpopulations were sufficient to drive the sorting of the

Dictyostelium slug. Yet the requirement that the overall cell density is constant prevents its application to earlier (preaggregated) phases of *Dictyostelium* development. Multi-phase models have also been developed to model biological tissues: the cell population(s), extracellular matrix, and water that make up a typical tissue are assumed to constitute the distinct components of a multi-phase mixture and the governing equations for their movement derive from mass and momentum balance considerations. In the context of cell movement, this approach has been utilized by Byrne and Owen (2004) to model chemotaxis and by Webb et al. (2007) to model the infiltration of macrophages into a solid tumor.

3. Derivation of the continuous model

The aim is to derive continuous models for movement in a heterogeneous (i.e., multiple cell-type) tissue. A discrete-space, continuous-time equation is initially postulated for the density of cells on a lattice before scaling to obtain a continuous macroscopic partial differential equation (PDE) model. Similar methods have been employed in a number of earlier models (e.g., Othmer and Stevens, 1997; Painter and Hillen, 2002; Painter and Sherratt, 2003) and, although biologically *naive*, it offers a simple path to the PDE system (the focus here). A rigorous derivation from a realistic individual model (e.g., an individual velocity-jump process; see Alt, 1980; Othmer et al., 1988; Hillen, 2002) is left for future work. As described above, an earlier attempt (Painter and Sherratt, 2003) using this method was only partially successful: the model captured the expected dependency on the populations in the movement terms, yet led to "population trapping" at high tissue densities, at odds with the behavior of certain populations (e.g., post-aggregation stages of *Dictyostelium*). As described earlier, movement of cells is contingent on their ability to anchor to an external substrate via adhesion complexes: For an isolated cell moving in a sparsely populated tissue, the forces can be directly transmitted to the surrounding extracellular matrix while for cells in a densely packed population with little extracellular material (e.g., *Dictyostelium* mound/slug) the adhesion complexes form with the neighboring cells. In this latter case, a cell can only pull itself forward by pulling other cells back, thus displacing its neighbor.

We assume a heterogeneous tissue composed of two cell types defined on a discrete 1D lattice of uniform spacing h. The densities of the two populations at x are denoted by U_x and V_x while $W_x = U_x + V_x$ defines the total cell density. We let $W_{\max}$ (= constant) represent the maximum tissue density; note that it would also be possible to allow this to vary in space. Setting $u_x = U_x / W_{\max}$, $v_x = V_x / W_{\max}$ and $w_x = W_x / W_{\max}$, u_x and v_x now represent the proportion occupied by each cell type at x while w_x and $1 - w_x$ represent the proportions of occupied/unoccupied space.

It is assumed that movement takes place either through movement unimpeded into neighboring unoccupied space or by an "active" cell (i.e., one that pulls forward) displacing a "passive" cell (i.e., one that is pulled back) in neighboring occupied space via a process of "location-swapping." For the two populations on a discrete 1D lattice of uniform spacing h, these give rise to the following three possibilities (schematically represented in Fig. 2):

(1) type u (or v) cells at x move into unoccupied space at $x \pm h$ with rate $P_x^{1\pm} u_x (1 - w_{x \pm h})$ (or $Q_x^{1\pm} v_x (1 - w_{x \pm h})$);
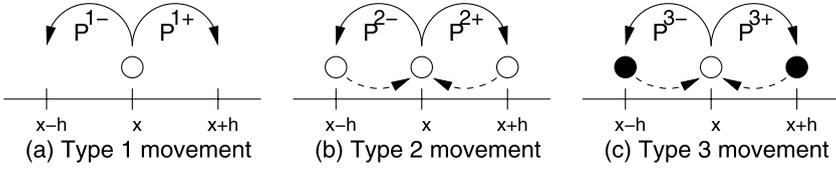
Fig. 2 Schematic showing the various movements allowed for an active cell at position x moving into (a) free space, (b) displacing a passive cell of *same type* at $x \pm h$ or (c) displacing a passive cell of *different type* at $x \pm h$.

(2) active type u (or v) cells at x displace passive type u (or v) cells at $x \pm h$ with rate $P_x^{2\pm} u_x u_{x\pm h}$ (or $Q_x^{2\pm} v_x v_{x\pm h}$);

(3) active type u (or v) cells at x displace passive type v (or u) cells at $x \pm h$ with rate $P_x^{3\pm} u_x v_{x\pm h}$ (or $Q_x^{3\pm} v_x u_{x\pm h}$).

The rate functions P, Q integrate the various factors impinging on the movement of the cells. Incorporating the above modes of movement, we obtain the following evolution equations for u and v at x:

$$
\begin{aligned}
\frac{du_x}{d\tau} =\ & +P_{x+h}^{1-} u_{x+h}(1 - w_x) + P_{x-h}^{1+} u_{x-h}(1 - w_x) - P_x^{1-} u_x(1 - w_{x-h}) \\
& - P_x^{1+} u_x(1 - w_{x+h}) + P_{x+h}^{3-} u_{x+h} v_x + P_{x-h}^{3+} u_{x-h} v_x \\
& - P_x^{3-} u_x v_{x-h} - P_x^{3+} u_x v_{x+h} \\
& - Q_{x+h}^{3-} v_{x+h} u_x - Q_{x-h}^{3+} v_{x-h} u_x + Q_x^{3-} v_x u_{x-h} + Q_x^{3+} v_x u_{x+h},
\end{aligned}
\tag{3a}
$$

$$
\begin{aligned}
\frac{dv_x}{d\tau} =\ & +Q_{x+h}^{1-} v_{x+h}(1 - w_x) + Q_{x-h}^{1+} v_{x-h}(1 - w_x) - Q_x^{1-} v_x(1 - w_{x-h}) \\
& - Q_x^{1+} v_x(1 - w_{x+h}) + Q_{x+h}^{3-} v_{x+h} u_x + Q_{x-h}^{3+} v_{x-h} u_x \\
& - Q_x^{3-} v_x u_{x-h} - Q_x^{3+} v_x u_{x+h} \\
& - P_{x+h}^{3-} u_{x+h} v_x - P_{x-h}^{3+} u_{x-h} v_x + P_x^{3-} u_x v_{x-h} + P_x^{3+} u_x v_{x+h}.
\end{aligned}
\tag{3b}
$$

In the equation for u, the first line corresponds to moves of type (1), the second to moves of type (3) in which active cells of type u displace passive cells of type v and the third to moves of type (3) in which active cells of type v displace passive cells of type u; note that moves of type (2) simply cancel. In the extension to 2D, we will assume a von Neumann neighborhood in which cells move to their 4 nearest neighbors on a square lattice; it is also possible to consider a Moore neighborhood composed of the 8 nearest neighbors.

To derive a fully continuous model, each of the functions $P^{1\pm,3\pm}$, $Q^{1\pm,3\pm}$ must be defined. *In vivo*, various guidance signals are integrated to orient the cell, for example, cell-cell interactions (adhesion, contact inhibition), the extracellular matrix (e.g., hapto-taxis, contact guidance) and extracellular signaling molecules such as chemotactic and chemokinetic cues. Here, the only guidance is assumed to stem from chemotaxis and cells bias movement according to a local chemical gradient:

$$
P_x^{\pm} \equiv Q_x^{\pm} \equiv k\big(1 + \kappa\,(a_{x\pm h} - a_x)\big),
\tag{4}
$$

where a represents the distribution of the chemotactic signal. k is a positive phenomenological constant which represents the "capacity for movement": this parameter would depend on a host of factors, principally the biochemical details surrounding the formation of adhesion complexes and biophysical properties regarding the local tissue environment. κ represents the ratio of chemotactic:random guidance. Note that the sign of κ can be positive or negative to describe chemoattraction or chemorepulsion. The above forms have been adopted in earlier derivations of chemotactic equations (e.g., Othmer and Stevens, 1997; Painter and Hillen, 2002): their employment here is motivated by their simplicity rather than strict biological accuracy.

3.1. Single cell population

Derivation of the macroscopic PDE from the discrete-space/continuous time Eq. (3) is straightforward: the process is illustrated following the restriction to a homogeneous tissue (i.e., a single cell population u). Setting $v = 0$ in Eqs. (3) we obtain

$$\frac{du_x}{d\tau} = \left(P_{x+h}^{1-}u_{x+h} + P_{x-h}^{1+}u_{x-h}\right)(1 - u_x) - u_x\left(P_x^{1-}(1 - u_{x-h}) - P_x^{1+}(1 - u_{x+h})\right)$$

with $P^{1\pm}$ given by Eq. (4). x is reinterpreted as a continuous variable, the RHS terms are expanded as Taylor's series and the scaling $\tau = \lambda t$ is introduced. Assuming that $\lim_{\lambda\to\infty,h\to0} k\lambda h^2 = D_u$, $\lim_{\lambda\to\infty,h\to0} 2k\kappa\lambda h^2 = \chi_u$ (where D_u, χ_u are constants) and extending the process to higher dimensions, we obtain the cell equation in the volume-filling model (2). Note that in the 2D derivation the same form of equation can also be derived when considering a Moore neighborhood (i.e., 8 nearest neighbors in the underlying discrete space model) although the precise forms for the limits vary.

3.2. Multiple cell populations

For two populations u and v, it is assumed that the movement properties are essentially the same:

$$P_x^{1\pm} = k_u^1\left(1 + \kappa_u(a_{x\pm h} - a_x)\right), \qquad P_x^{3\pm} = k_u^3\left(1 + \kappa_u(a_{x\pm h} - a_x)\right),$$
$$Q_x^{1\pm} = k_v^1\left(1 + \kappa_v(a_{x\pm h} - a_x)\right), \qquad Q_x^{3\pm} = k_v^3\left(1 + \kappa_v(a_{x\pm h} - a_x)\right). \tag{5}$$

As earlier, each of the k^1's are constant parameters for the capacity of movement within uncrowded regions, while the k^3's are the corresponding parameters for crowded regions: *in vivo* these parameters would depend on the capacity of the cells to bind to either other cells or the substrate. Substituting (5) into Eqs. (3), deriving the PDE model and extending to higher dimensions gives the two-population model:

$$\frac{\partial u}{\partial t} = \overbrace{\alpha_u\nabla\left((1 - w)\nabla u + u\nabla w\right)}^{(1u)} + \overbrace{(\beta_u + \beta_v)\nabla(v\nabla u - u\nabla v)}^{(2u)}$$
$$- \underbrace{\alpha_u\phi_u\nabla\left((1 - w)u\nabla a\right)}_{(3u)} - \underbrace{(\beta_u\phi_u - \beta_v\phi_v)\nabla(uv\nabla a)}_{(4u)}, \tag{6a}$$

Table 1 List of the parameters and their interpretations for Eqs. (6)

Parameter	Definition
$\alpha_u(\alpha_v)$	Random motility coefficient of populations u (v) in uncrowded regions. Note that this parameter corresponds to the cell diffusion coefficient in dispersed populations
$\beta_u(\beta_v)$	Random motility coefficient of populations u (v) in crowded regions
$\alpha_u\phi_u(\alpha_v\phi_v)$	Chemotactic efficiency of population u (v) within uncrowded regions
$\beta_u\phi_u(\beta_v\phi_v)$	Chemotactic efficiency of population u (v) within crowded regions

$$\frac{\partial v}{\partial t} = \overbrace{\alpha_v \nabla((1-w)\nabla v + v\nabla w)}^{(1v)} + \overbrace{(\beta_u + \beta_v)\nabla(u\nabla v - v\nabla u)}^{(2v)}$$

$$- \overbrace{\alpha_v \phi_v \nabla\big((1-w)v\nabla a\big)}^{(3v)} - \overbrace{(\beta_v\phi_v - \beta_u\phi_u)\nabla(uv\nabla a)}^{(4v)}, \tag{6b}$$

where $\alpha_{u,v} = \lim_{\lambda\to\infty,h\to 0} k^1_{u,v}\lambda h^2$, $\beta_{u,v} = \lim_{\lambda\to\infty,h\to 0} k^3_{u,v}\lambda h^2$, $\phi_{u,v} = \lim_{\lambda\to\infty,h\to 0} 2\kappa_{u,v}\lambda h^2$. A list of the parameters and their interpretations is provided in Table 1. The RHS terms in the above equations break down as:

- terms (1u) (or (1v)) derive from the random (i.e., diffusive) motility of cells u (or v) in uncrowded regions (i.e., movement of type (1) in Fig. 2) with uncrowded random motility coefficient α_u (or α_v);
- terms (2u) (or (2v)) arise from the random component in which active u (or v) cells displace passive cells of type v (or u) (i.e., movement of type (3) in Fig. 2) with crowded random motility coefficient β_u (or β_v);
- terms (3u) (or (3v)) follow from the chemotactic component to movement of cells u (or v) in uncrowded regions with uncrowded chemotactic efficiency $\alpha_u\phi_u$ (or $\alpha_v\phi_v$);
- terms (4u) (or (4v)) derive from the chemotactic component to the movement in which active cells of type u (or v) displace passive cells of type v (or u) with crowded chemotactic efficiency $\beta_u\phi_u$ (or $\beta_v\phi_v$).

Adding Eqs. (6) gives the evolution equation for the total cell distribution:

$$\frac{\partial w}{\partial t} = \nabla\big((1-w)(\alpha_u\nabla u + \alpha_v\nabla v) + (\alpha_u u + \alpha_v v)\nabla w\big)$$

$$- \nabla\big((1-w)(\alpha_u\phi_u u + \alpha_v\phi_v v)\nabla a\big). \tag{7}$$

As should be expected, the terms in (7) only derive from migration in uncrowded regions: Movement through displacement has no bearing on the total cell density.

The aim is to explore the capacity of Eq. (6) to model different types of movement in both crowded (dense) and uncrowded (dispersed) tissues. To concentrate solely on the movement terms, we dispense of cell kinetics, though note that cell growth, death or transdifferentiation between the two cell types can easily be incorporated. Realistic initial conditions require $0 \le u(x,0), v(x,0) \le w(x,0) \le 1$: cell densities are neither negative nor exceed the maximum tissue density. For the signal kinetics, both an independent

chemotactic signal profile and the following two-population extension of the linear signal dynamics in Eqs. (2) are considered:

$$\frac{\partial a}{\partial t} = D_a \nabla^2 a + \mu u + \nu v - \delta a, \tag{8}$$

where μ and ν represent the rates of signal production by u and v respectively, D_a is the chemical diffusion coefficient and δ represents chemical degradation: The focus here is on patterning via cell interactions and linear signaling kinetics are chosen for their simplicity.

4. Migration in crowded/uncrowded tissues

4.1. Migration in a crowded tissue

For a crowded tissue, it is assumed that the extracellular space between cells is minimal; for example, mound and slug stages in *Dictyostelium*, epithelial tissues or certain types of solid tumor. Therefore $w(x, 0) = 1$ and, via Eq. (7), $w(x, t) = 1$ for $t > 0$. This conservation law allows the reduction of Eqs. (6) to a single cell equation by setting $v = 1 - u$, resulting in the *crowded-tissue model*:

$$\frac{\partial u}{\partial t} = \nabla\big((\beta_u + \beta_v)\nabla u - (\beta_u \phi_u - \beta_v \phi_v)u(1 - u)\nabla a\big) \quad \text{and} \quad \frac{\partial u}{\partial t} = -\frac{\partial v}{\partial t}. \tag{9}$$

Thus, the movement of u is exactly countered by that of v to maintain uniform total density: the above equations are similar to those employed by Pate and Othmer (1986) to describe prespore and prestalk patterning within the *Dictyostelium* slug. Note further that the above two-equation system reduces to the single cell volume-filling model (2). In the special case of symmetric populations (i.e., both populations equally efficient), $\beta_u \phi_u = \beta_v \phi_v$ and all tactic terms disappear. The properties of Eqs. (9) can be understood by examining two scenarios: a response by cells to a fixed gradient and an autocrine process in which cells produce their own chemotactic signal.[1]

4.1.1. Fixed gradient
Here, it is assumed that a chemoattractant diffuses through the tissue from a source (at $x = 0$) to create the fixed profile

$$a(x) = a_0 \exp(-\theta x), \tag{10}$$

where a_0, θ are positive parameters. The signal is presumed to be an attractant for both u and v with u the more efficient population: $\beta_u \phi_u > \beta_v \phi_v > 0$. Initially, u is placed further away from the source:

$$u(x, 0) = \big(1 + \tanh(x_1(x - x_0))\big)/2 \quad \text{and}$$
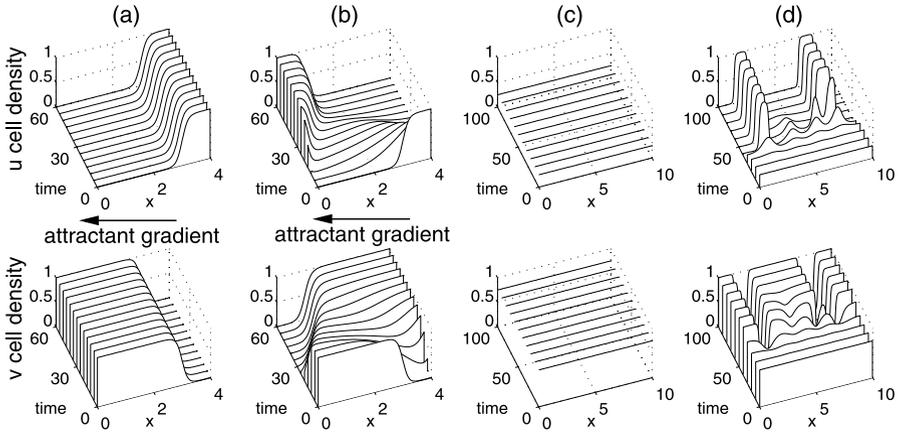$$v(x, 0) = 1 - u(x, 0) = \big(1 - \tanh(x_1(x - x_0))\big)/2.$$

Fig. 3 Simulations of population movement in a crowded and heterogeneous tissue. (a)/(b) Response to a fixed attractant gradient (direction of increasing attractant indicated by arrow). In (a) it is assumed that there is no movement by displacement ($\beta_{u,v} = 0$) and populations u (top row) and v (bottom row) are immobilized: the more efficient population (u) remains trapped further from the chemotactic source. In (b), cell displacement occurs ($\beta_{u,v} = 0.01$) and the more efficient population (u) is able to displace the weaker one at the attractant source. For both (a) and (b), Eqs. (9) were solved with a given by (10) on the domain [0, 4] subject to the stated initial/boundary conditions with $x_0 = 3$, $x_1 = 5$, $a_0 = 1$, $\theta = 0.25$ and $\phi_u = 200$, $\phi_v = 100$. (c)/(d) Cells produce the chemotactic signal. In (c) $\beta_{u,v} = 0$ and the populations are again immobilized: cells remain at the quasi-uniform initial distribution. In (d) $\beta_{u,v} = 0.01$ and cell migration can continue within the crowded tissue. Chemotactic sorting occurs provided condition (12) is satisfied and the two populations separate into distinct spatial compartments. For (c) and (d), Eqs. (11) were solved numerically on the 1D domain [0, 10] subject to periodic boundary conditions with $u(x, 0) = 0.25 + r(x)$, $v(x, 0) = 1 - u(x, 0)$ (where $r(x)$ is a small (1%) random spatial perturbation) and $a(x, 0)$ set at its steady state value. Other parameters were set at $\phi_u = 200$, $\phi_v = 100$ and $\rho = 0.0$. Simulations were performed as described in the Appendix with $\Delta x = 0.02$ in (a) and (b) and $\Delta x = 0.05$ in (c) and (d).

Equations (9) with $a(x)$ given by (10) are solved on a 1D domain [0, L] subject to zero-flux boundaries conditions.

For cells *unable* to move in crowded tissues ($\beta_u = \beta_v = 0$), the RHS terms in Eqs. (9) vanish and the solutions are trivial. No movement is possible and u is trapped away from the chemotactic source (Fig. 3(a)). Immobilization of a motile cell population as a result of close packing may be applicable in certain systems, yet is certainly not universally valid. Allowing cells to move in a crowded tissue (at least one of $\beta_{u,v} > 0$), permits migration to continue (Fig. 3(b)) and, as the more efficient population, the net movement of u is up gradients in a resulting in its displacement of v at the attractant source. Increasing the size of $\beta_u \phi_u - \beta_v \phi_v$ accelerates this process.

4.1.2. Autotactic responses
The analysis is expanded to explore the conditions under which a heterogeneous and packed tissue can spatially sort via differential chemotactic responses. Equations (9) are coupled to the signal dynamics (8) (with $v = 1 - u$) and (without loss of generality) u

---

[1]Note that while the model considers minimal extracellular space, it is implicitly assumed that there is enough space between cells for small extracellular molecules to pass.

is assumed to produce chemical ($\mu > 0$) and at a greater (or equal) rate to v ($v \le \mu$). Introducing the scalings

$$\hat{t} = \delta t, \qquad \hat{\mathbf{x}} = \sqrt{\frac{\delta}{D_a}} \mathbf{x}, \qquad \hat{a} = \frac{\delta}{\mu} a, \qquad D = \frac{(\beta_u + \beta_v)}{D_a},$$

$$\chi = \frac{\mu(\beta_u \phi_u - \beta_v \phi_v)}{D_a \delta}, \qquad \rho = \frac{v}{\mu},$$

generates the following nondimensional equations (after dropping the "hats")

$$\frac{\partial u}{\partial t} = D\nabla^2 u - \chi\nabla\big(u(1-u)\nabla a\big), \tag{11a}$$

$$\frac{\partial a}{\partial t} = \nabla^2 a + \rho + (1-\rho)u - a. \tag{11b}$$

Note that $0 \le \rho \le 1$ and $D \ge 0$. The above are studied on a 1D ($[0, L]$) domain subject to periodic boundary conditions and realistic initial conditions ($u(x, 0) \in [0, 1]$). The model (11) is equivalent to the volume-filling model (2) derived previously in Painter and Hillen (2002) and possesses the uniform steady state $(u_s, v_s) = (u_s, \rho + u_s(1 - \rho))$ (where $u_s \in [0, 1]$ follows from the initial data). Linear stability analysis determines the instability condition

$$\chi(1 - \rho) > \frac{D}{u_s(1 - u_s)}. \tag{12}$$

The above implies $\chi > 0$ and $\rho \ne 1$ for patterning to occur: sorting requires the cell populations to have *both* different chemotactic responses *and* different rates of signal production. Further, patterning may occur even when the signal acts as a repellent for both u and v. With $\beta_u = \beta_v = 0$ (no movement in crowded tissues), $\chi = D = 0$ and the RHS terms in (11a) vanish: patterning will not occur and the cell populations remain immobilized (see Fig. 3(c)). For at least one of $\beta_{u,v} > 0$ (with condition (12) met) sorting of the tissue into compartmentalized populations can occur (e.g., see Fig. 3(d)).

4.2. Migration in uncrowded tissues

We assume next that a significant portion of unoccupied space exists between the cells: $w_0 < 1$ where w_0 is the spatially averaged proportion of occupied space. To reduce the number of parameters for the study, it will be assumed the two cell types are identical with the exception of their chemotactic efficiency: Therefore, $\alpha_u = \alpha_v = \alpha$ and $\beta_u = \beta_v = \beta$ in Eqs. (6), i.e., the capacities for movement for the two cell types are the same. The following three general cases will be investigated:

1. Movement takes place only by displacement of other cells, $\alpha = 0$, $\beta > 0$ (i.e., only moves of types (2)/(3) in Fig. 2);
2. Movement takes place only through moving into free space, $\alpha > 0$, $\beta = 0$ (i.e., only moves of type (1) in Fig. 2);
3. Cells equally adept at moving into free space/moving through displacement, $\alpha = \beta > 0$.
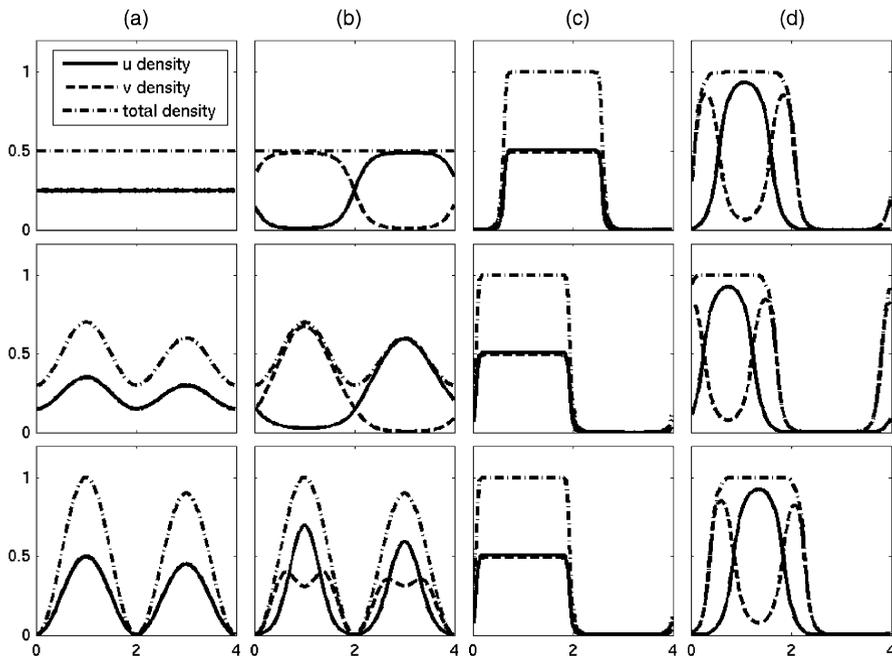
Fig. 4 Tissue and subpopulation movement in a heterogeneous tissue. Initially, the tissue is distributed according to one of the three configurations indicated in column (a) (note that initially the u and v subpopulations are almost equally distributed). (b) $\alpha = 0.0, \beta = 0.01$. Movement only occurs by displacement and the distribution of the tissue remains unchanged. Within-tissue redistribution results in the sorting of population u from population v. (c) $\alpha = 0.01, \beta = 0.0$. Movement only into free space and the tissue accumulates into a single aggregate. No within-tissue sorting of the populations can occur. (d) $\alpha = \beta = 0.01$. A single aggregation develops in which the distinct subpopulations spatially sort, eventually forming an "engulfed" pattern. Other parameters are set at $\phi_u = 200.0, \phi_v = 100.0, D_a = \mu = \delta = 1.0$ and $v = 0.0$. Equations (6) with (8) were solved on a 1D domain [0, 4] as described in the Appendix using $\Delta x = 0.04$ and periodic boundary conditions. Note that in the first row, aggregations develop at a random location due to the noise in the initial data. For the bottom two rows the positions of aggregations are determined by the bias in the initial cell distribution.

The first is applicable to cells unable to attach to an extracellular surface/substrate. In this case, as argued earlier, we should expect no *tissue-level* movement to occur. The second models populations unable to develop physical attachments with other cells (i.e., unable to form cell-cell adhesions)—at high cell densities (close to the maximum density), we expect within tissue movement to be highly restricted. Equations (6) are coupled to the linear signal kinetics (8) and studied numerically subject to three distinct initial configurations (illustrated in Fig. 4 column (a)): an initially uniform tissue (top row) and nonuniform tissues (middle and bottom rows). Note that the initial distributions of the subpopulations u and v are the same (subject to a small random perturbation). In the simulations shown in Fig. 4, u is the only signal secreter ($v = 0$) and displays greater chemotactic efficiency ($\phi_u > \phi_v$). The equations are numerically solved until solutions have evolved to a heterogeneous steady state distribution (as defined in the Appendix).

For (1) movement only by displacement, cells are unable to migrate into unoccupied space: $\alpha = 0$ in Eq. (7) implies that the total cell density is fixed. As expected, the net movement of the tissue in this case is zero (Fig. 4(b)). Within the tissue, however, subpopulations move via displacement and differential chemotaxis permits within-tissue sorting of the two populations similar to that previously observed. Note that for the initial distribution in the bottom row, the total cell density at the troughs is zero and no transfer from one peak to the other occurs: This is reflected in both subpopulations being present in each of the peaks.

For (2), $\alpha > 0$ and the total cell density will vary over time: The capacity for cells to migrate into free space enables movement of the entire tissue and chemotaxis drives aggregation into a single mound; see Fig. 4(c). However, inside the mound $w \lesssim 1$, and since $\beta = 0$, from Eqs. (6), we expect restricted movement of the subpopulations. This is reflected in the lack of within-tissue sorting of the subpopulations.

For (3), by combining both movement by displacement and into free space, an amalgamation of the above results is observed: Movement into free space results in tissue level patterning (evolution into a single aggregation) while movement by displacement allows within-tissue sorting of the subpopulations into distinct compartments. For the chosen parameters, this results in the formation of an "engulfed" distribution in which the more efficient/signal producing population (u) is focused to the center and the less efficient one (v) is confined to the periphery (Fig. 4(d)). Note that the initial distribution does not notably alter the configuration of the population. Further note that in these simulations we have conveniently set $\alpha = \beta$; choosing $\alpha > \beta$ (i.e., movement into free space is "easier" than movement by displacement) or $\beta > \alpha$ (movement by displacement is "easier" than movement into free space) does not greatly alter the final pattern, but does impact on the timing of the various patterning processes.

In this section, it was shown that the model is capable of describing movements of and within a heterogeneous tissue: different assumptions on the capacity of the populations to move markedly alter the different types of patterning observed. In Fig. 4(d), the populations sorted into an engulfed distribution, analogous to those observed for adhesion driven sorting (e.g., Foty and Steinberg, 2004; Armstrong et al., 2006). The parameters for α and β were identical, and thus the patterning can be attributed to the different chemotactic efficiencies. In the next section, the extent to which differential chemotaxis can spatially organize a heterogeneous tissue is investigated further.

5. Cell sorting via differential chemotaxis

Population displacement and distinct responses to a chemotactic signal were shown above to drive within-tissue sorting of distinct subpopulations. The distinct motility responses of prespore and pre-stalk cells (Early et al., 1995) appears to play a key role during *Dictyostelium* sorting and differential chemotaxis has been postulated as a mechanism for this process (Matsukuma and Durston, 1979). A variety of theoretical models support this theory (e.g., Pate and Othmer, 1986; Vasiev and Weijer, 1999; Palsson and Othmer, 2000; Umeda and Inouye, 2004).

While experimental (reviewed in Foty and Steinberg, 2004; Steinberg, 2007) and theoretical (e.g., Glazier and Graner, 1993; Armstrong et al., 2006) studies have explored the
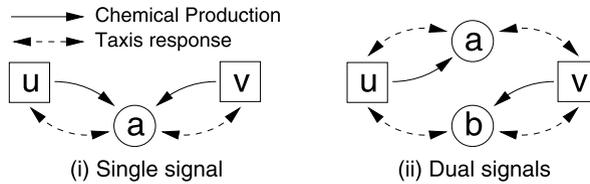
Fig. 5 Illustration of the two sorting scenarios. (i) Two cell populations (u and v) both produce and respond to a single signal (a). (ii) The two cell populations (u and v) each produce a distinct chemotactic signal (a and b).

capacity for *differential-adhesion* to sort tissues, a detailed investigation into differential-chemotaxis induced patterning is lacking. We use the model to initiate this study here, comparing the results with those obtained via differential-adhesion. A heterogeneous tissue is considered comprised of two populations (u and v) exhibiting one of the following interactions (see also Fig. 5):

- a single chemotactic signal produced by both populations (Fig. 5(i)),
- dual chemotactic signals, each produced by a distinct cell population (Fig. 5(ii)).

The former is relevant to *Dictyostelium* mound patterning, although we do not intend to directly model this system: any applications would require careful consideration of appropriate signaling dynamics. Multiple tactic signals have been identified as playing a role in the patterning of a number of biological systems, for example, a combination of attraction to FGF4 and repulsion by FGF8 directs primitive streak cells during chick gastrulation (Yang et al., 2002).

Comparing with differential-adhesion, a single signal can be likened to two populations presenting the same type of adhesion receptor at their membrane, albeit at varying densities: the populations will be intrinsically linked through their production of/response to the same signal. The latter scenario (dual signals) can be compared with two populations presenting multiple classes of adhesion receptors at varying concentrations: The interactions between the populations will depend on their precise response to the different signals. This analogy indicates similar patterning can be expected, yet certain differences demand remark. Firstly, chemotactic responses can be either attractive or repulsive while adhesion is strictly attractive. Secondly, for differential adhesion, the cross-population interactions are symmetric since adhesive binding between the two separate cell types will generate equal but opposite forces. For differential chemotaxis, this symmetry vanishes: the response of u to the signal produced by v is likely to be different to that of v to the signal produced by u.

5.1. Sorting under a single signal

The single signal case expands the study in Section 4. Thus, equations for cell movement are given by (6) while the chemical dynamics are given by (8). In Section 4, it was demonstrated that distinct chemotactic responses could lead to the within tissue sorting of subpopulations in a crowded tissue (see Fig. 3(d)) and to the engulfment of one population by the other in the case of an uncrowded tissue (see Fig. 4(d)). The focus of this study is to determine the range of patterning that can be induced via differential chemotaxis and,

to focus on the relevant parameters, it is therefore assumed that the two cell populations are equivalent with the exception of their chemotactic sensitivities with both populations equally adept at moving in crowded/uncrowded regions:

$$\alpha_u = \alpha_v = \beta_u = \beta_v \equiv \alpha. \tag{13}$$

The above restriction both reduces the number of free parameters and simplifies the equations. The behavior reported in the following sections can also be observed when restriction (13) is lifted, although a thorough analysis has not been conducted. As before, it is assumed that $\mu > 0$ and $0 \leq \nu \leq \mu$ in Eqs. (8). By setting (13) in Eqs. (6) and introducing the scalings

$$\hat{t} = \delta t, \qquad \hat{\mathbf{x}} = \sqrt{\frac{D_a}{\delta}} \mathbf{x}, \qquad \hat{a} = \frac{\delta}{\mu} a, \qquad D = \frac{\alpha}{D_a},$$

$$\chi_u = \frac{\alpha \phi_u \mu}{D_a \delta}, \qquad \chi_v = \frac{\alpha \phi_v \mu}{D_a \delta}, \qquad \rho = \frac{\nu}{\mu},$$

we arrive at the nondimensional system (after dropping the "hats")

$$\frac{\partial u}{\partial t} = D\nabla\big((1+v)\nabla u\big) - D\nabla(u\nabla v) - \chi_u \nabla\big(u(1-u)\nabla a\big) + \chi_v \nabla(uv\nabla a), \tag{14a}$$

$$\frac{\partial v}{\partial t} = D\nabla\big((1+u)\nabla v\big) - D\nabla(v\nabla u) - \chi_v \nabla\big(v(1-v)\nabla a\big) + \chi_u \nabla(uv\nabla a), \tag{14b}$$

$$\frac{\partial a}{\partial t} = \nabla^2 a + u + \rho v - a. \tag{14c}$$

Note that $0 \leq \rho \leq 1$. In the above, the populations differ only with respect to their chemotactic efficiencies (χ_u and χ_v) to a and rate of signal production (ρ). Equations (14) will be studied on both a 1D domain $[0, L]$ and 2D square $[0, L] \times [0, L]$ with periodic boundary conditions. Initially, a uniform total cell density $w(x, 0) = w_0$ is considered, composed of an equal mixture of the 2 cell types. Specifically,

$$u(\mathbf{x}, 0) = w_0/2 + \Phi(\mathbf{x}) \quad \text{and} \quad v(\mathbf{x}, 0) = w_0/2 - \Phi(\mathbf{x}),$$

where $\Phi(\mathbf{x})$ is a small random perturbation, normalized such that the spatially averaged cell densities are both equal to $w_0/2$. The above ensures that the two cell populations are uniformly distributed throughout the tissue, thus modeling the initial dispersing and random mixing of the subpopulations.

5.1.1. Numerical analysis

A linear stability analysis of the 1D case about its homogeneous steady state determines the following third order characteristic polynomial for the eigenvalues λ:

$$0 = \lambda^3 + a(k^2)\lambda^2 + b(k^2)\lambda + c(k^2), \quad \text{with} \tag{15}$$

$$a(k^2) = 2\big(1 + k^2(Dw_0 + 2D + 1)\big),$$

$$b(k^2) = k^2\big(D\big(2 + D + w_0(1 + D)\big)k^2 + \big(D(2 + w_0)$$
$$+ \, w_0^2(1 + \rho)(\chi_u + \chi_v)/4 - w_0(\chi_u + \rho\chi_v)/2\big)\big),$$
$$c(k^2) = k^4\big(D^2(1 + w_0)k^2 + D\big(D(1 + w_0)$$
$$+ \, w_0^3(\chi_u + \chi_v)(1 + \rho)/4 - w_0(\chi_u + \rho\chi_v)/2\big)\big),$$

where k is the wavenumber. A complete analysis into the conditions under which at least one of the eigenvalues has a positive real component (and hence instability of the steady state) is algebraically intricate and outside the aims of the present paper: We remark only that instability will depend on the sizes/signs of the above coefficients and hence on the sizes of the chemotactic sensitivities. Instead, a numerical analysis into the properties of Eqs. (14) is employed. We set $D = 0.01$ as an appropriate value (i.e., random cell motility is two orders of magnitude slower than chemical diffusion), and assume the χ's are restricted to the ranges

$$-2 \leq \chi_u, \chi_v \leq 2.$$

Solutions are obtained through numerical integration of (14) until solutions have either converged to a stationary solution (defined numerically) or a maximum upper time limit is reached (see the Appendix for details). Note that we cannot determine whether the solutions obtained numerically represent stationary solutions or slowly-evolving transients. Indeed, either possibility is conceivable within chemotactic systems (e.g. Hillen and Painter, 2009). Comprehensively addressing these issues would require nonlinear analysis, outside the aim of the present work.

A systematic exploration of the (χ_u, χ_v, ρ) parameter space was conducted, revealing three major behavior types: *no patterning* (solutions evolved to the uniform steady state), *stationary patterns* (solutions evolve to a nonuniform steady-state distribution), and *temporal patterns* (nonuniform solutions undergoing sustained temporal dynamics). The second and third types can be further subclassified according to the spatial arrangement of cell populations or the form of the temporal behavior. Using the same terminology as introduced for adhesion-driven sorting (see Fig. 1), for the stationary patterns

(a) *Single population aggregations* (one population aggregated, other remains dispersed, Fig. 6(a));
(b) *Complete sorting* (subpopulations organize into separate aggregations for u and v, Fig. 6(b));
(c) *Engulfment* (single aggregation with one subpopulation enclosed by the other, Fig. 6(c));
(d) *Mixing* (single aggregation forms with no within-aggregation sorting of u and v, Fig. 6(d)).

Each of the above classes are robust with respect to the initial total cell density (rows in Fig. 6(i)). Only in the limiting scenario $w_0 = 1.0$ do the pattern classes become indistinguishable: for $w_0 = 1$, Eqs. (14) revert to the crowded tissue model and the only patterns are mixing or compartmentalization of u and v within the tissue (see Section 4.1.2). On a larger domain, separate and sorted aggregations initially develop which subsequently coarsen (as observed previously for single-population chemotaxis models, e.g., Hillen and Painter, 2009). This is shown in Fig. 6(iii) for the "engulfment" class.
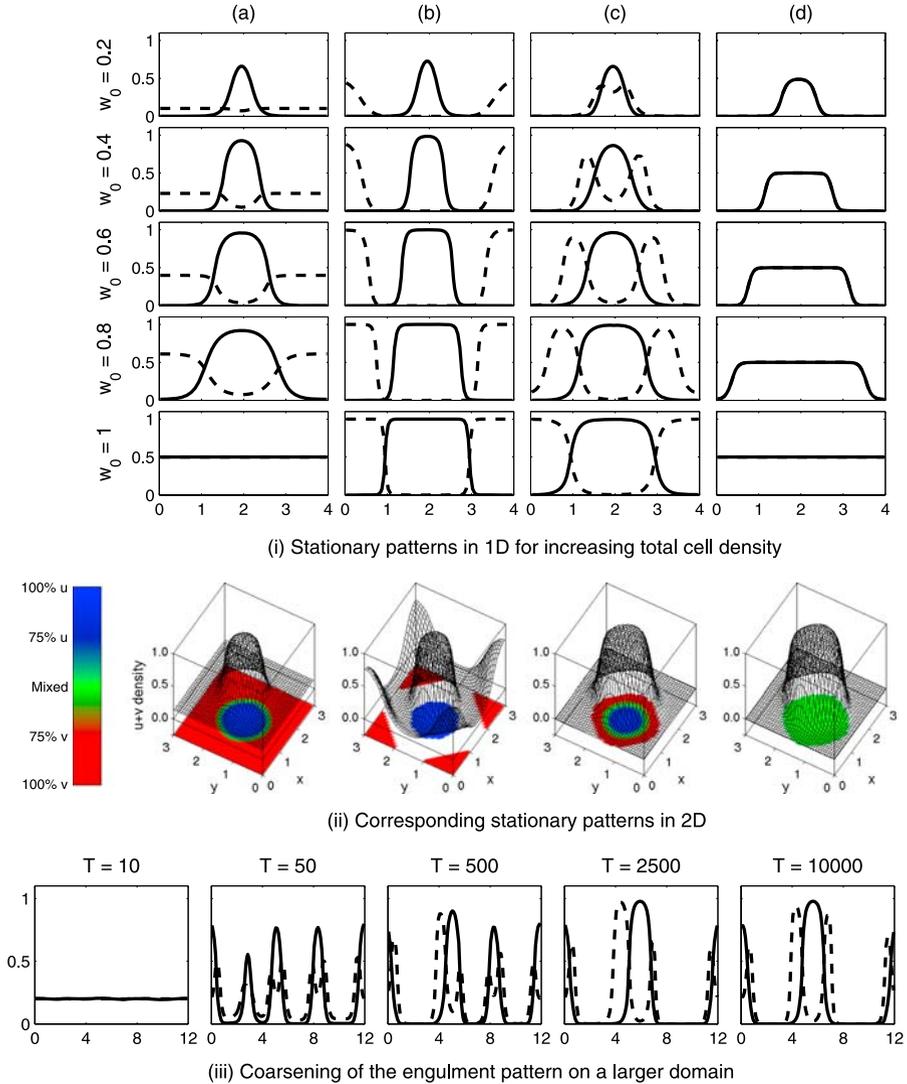
(i) Stationary patterns in 1D for increasing total cell density

(ii) Corresponding stationary patterns in 2D

(iii) Coarsening of the engulment pattern on a larger domain

Fig. 6 (i) Examples of the 4 classes of stationary pattern found for Eqs. (14). The distributions of u (solid line) and v (dashed line) are shown for (a) *single population aggregates* $(\chi_u, \chi_v, \rho) = (1, 0, 1)$, (b) *complete sorting* $(1, -2, 0)$, (c) *engulfment* $(2, 1, 1)$, and (d) *mixing* $(1, 1, 1)$. Note that in (d) the distributions of u and v are indistinguishable. From top to bottom, the initial total cell density is increased from 0.2 to 1.0. (ii) Corresponding stationary patterns on a 2D square domain. The distributions in 2D are represented by plotting the total $(u + v)$ density (black mesh) and representing the proportions of u and v within the aggregation by the underlying colorplot (regions with low total cell density are shaded white for clarity). In the 2D simulations $w_0 = 0.25$. (iii) Coarsening of the engulfment pattern on a larger initial domain. The populations initially aggregate into multiple aggregations which merge over time. In the above simulations, Eqs. (14) were solved as described in the Appendix on the domains (i) $[0, 4]$ ($\Delta x = 0.05$), (ii) $[0, 3] \times [0, 3]$ ($\Delta x = \Delta y = 0.04$) and (iii) $[0, 12]$ ($\Delta x = 0.1$) with periodic boundary conditions.
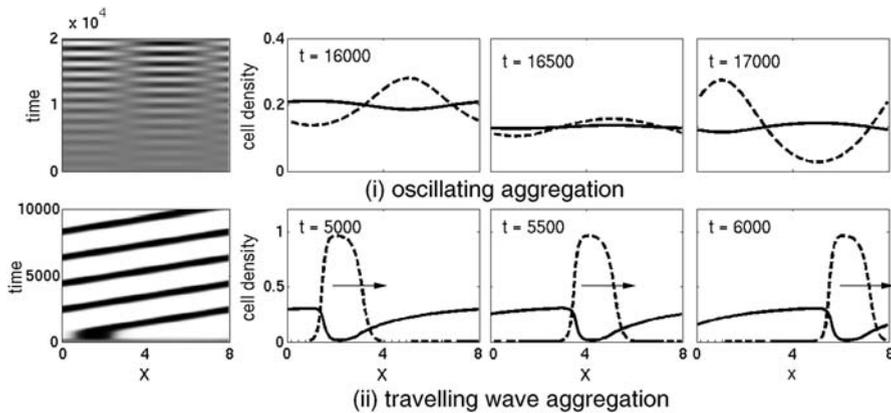
Fig. 7 Examples of sustained spatio-temporal patterning in the one-signal model. (i) *Oscillating aggregation*. The left-most frame gives the "space-time plot" (black indicates a higher proportion of v-cells, white indicates a higher proportion of u cells) and the other frames show snapshots of the spatial distribution for u (solid line) and v (dashed) at the indicated times. (ii) *Traveling aggregation* (moving with constant speed/shape in the direction indicated by the arrow). Equations (14) were solved on the 1D domain [0, 8] for (i) $\chi_v = -2.0$ and (ii) $\chi_v = -1.0$ with remaining parameters set at $\chi_u = \nu = 0.0$ and $w_0 = 0.4$. For each of the above simulations, Eqs. (14) were solved as described in the Appendix on the domain (i) [0, 8] ($\Delta x = 0.1$) and periodic boundary conditions.

Two classes of sustained spatio-temporal dynamics were identified:

(a) *Oscillating aggregations*—aggregations undergo sustained oscillations (Fig. 7(i));
(b) *Traveling aggregations*—traveling wave in the form of a migrating aggregation (Fig. 7(ii)).

It is worth remarking that oscillating aggregations have also been reported in a 3 variable chemotaxis models by Painter and Hillen (2002); however, for a single cell population responding to two chemical signals.

5.1.2. Patterning in the (χ_u, χ_v, ρ) space

The correlation between chemotactic efficiency and pattern type was investigated by systematic exploration of (χ_u, χ_v, ρ) space. Equations (14) were numerically solved at different (χ_u, χ_v) points and fixed ρ and the pattern was classified at the end of each run. The plots in Fig. 8 display the results for (a) $\rho = 1$ (populations produce equal amounts of signal) and (b) $\rho = 0$ (only u produces signal). Simulations at intermediate values of ρ reveal interlying behavior.

Explicit calculation of the dispersion relation (15) at each parameter set revealed a range of positive wavenumbers with a positive and real eigenvalue for locations giving rise to stationary patterns and eigenvalues with both positive real and nonzero imaginary parts at locations giving rise to spatio-temporal patterns. When $\rho = 1$ (Fig. 8(a)), the patterning is symmetric about the diagonal and no temporal behavior is observed. The following general relationships were observed:

- *Single aggregation peaks generally occur for $\chi_u > 0$, $\chi_v = 0$ (or vice versa)*. Here, aggregation of the chemotactic population occurs through signal production/chemoattrac-
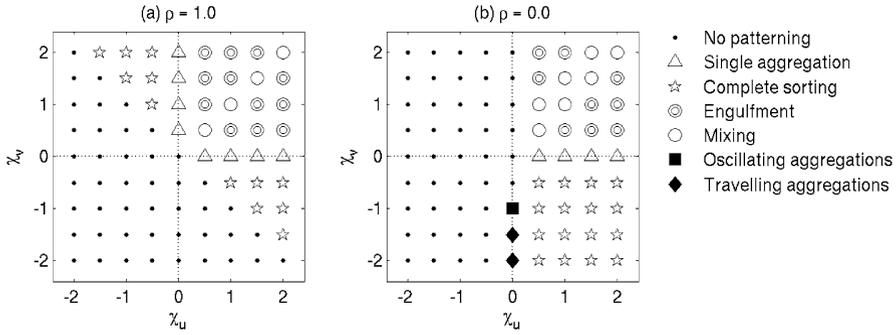
Fig. 8 Variation of pattern type with chemotactic efficiencies for Eqs. (14) when (a) $\rho = 1$ and (b) $\rho = 0$. Equations (14) were solved as described in the Appendix on a 1D domain $[0, 4]$ (using $\Delta x = 0.05$ and periodic boundary conditions).

tion feedback. The nontactic population is displaced from the region occupied by the aggregation and remains dispersed.

- *Complete sorting occurs for* $\chi_u > 0 > \chi_v$ *(or* $\chi_v > 0 > \chi_u$*)*. The signal production/positive chemotaxis feedback creates the primary aggregation of one population while the chemorepulsive response of the second population forces them into a separate aggregation mound.
- *Engulfment occurs for* $\chi_u > \chi_v > 0$ *(or* $\chi_v > \chi_u > 0$*)*. The positive chemotaxis by both populations result in a single aggregation. The more sensitive population accumulates at the center (corresponding to the chemoattractant peak) through its displacement of the less sensitive population.
- *Mixing occurs for* $\chi_u \sim \chi_v > 0$. With positive and similar chemotactic sensitivities, aggregation into a mound occurs yet the small difference in chemotactic sensitivities prevents any within-mound sorting of the subpopulations.

When $\rho = 0$ (Fig. 8(b)) similar relationships define the patterns, yet asymmetry in the production rate rotates the patterning into the $\chi_u > 0$ region. Note further that sustained temporal patterns can develop (as illustrated in Fig. 7). Patterning in this instance derives from the aggregation of v into a mound through its repulsion from the signal produced by u. However, it is worth stressing that the temporal behavior observed was only found in restricted parameter regions and was highly sensitive to both domain size and initial conditions.

Above, we demonstrated that a single chemotactic signal can generate a wide variety of patterning in a heterogeneous tissue. Comparing with differential-adhesion, earlier we likened the single signal case to two cell populations displaying the same class of adhesion receptor (albeit at different concentrations): in differential-adhesion only attractive responses are possible and, therefore, only mixing or engulfment can be expected. With differential-chemotaxis, positive and negative responses extend the patterning to include complete sorting and temporal patterns. Further, we note that only simple kinetics have been considered here: chemotactic populations may also regulate degradation of the signal, possibly leading to a greater range of patterning.

5.2. *Sorting behavior under two signals*

The analysis is extended such that populations u and v each generate distinct chemotactic signals (a and b respectively) that elicit chemotactic responses from both populations. Thus, each of u and v display both a *self-taxis* (to a and b) and *cross-taxis* (to b and a) response. The derivation of Eqs. (6) assumed a single chemotactic cue yet extension to multiple chemotactic signals is straightforward (e.g., see Painter et al., 2000; Luca et al., 2003). Specifically, functions (5) are assumed to incorporate biases to local gradients in a and b:

$$P, Q \equiv k\big(1 + \kappa_a(a_{x\pm h} - a_x) + \kappa_b(b_{x\pm h} - b_x)\big).$$

The derivation of the macroscopic model follows as for Eqs. (6) and, after incorporating linear chemical kinetics, employing the same assumptions as given by (13) and nondimensionalizing, the following model is derived (see the Appendix for full details):

$$\frac{\partial u}{\partial t} = \nabla\Big(\overbrace{D(1+v)\nabla u - Du\nabla v}^{(1u)} - \overbrace{u(1-u)(\chi_{u-a}\nabla a + \chi_{u-b}\nabla b)}^{(2u)}$$

$$+ \overbrace{uv(\chi_{v-a}\nabla a + \chi_{v-b}\nabla b)}^{(3u)}\Big), \tag{16a}$$

$$\frac{\partial v}{\partial t} = \nabla\Big(D(1+u)\nabla v - Dv\nabla u - v(1-v)(\chi_{v-a}\nabla a - \chi_{v-b}\nabla b)$$

$$+ uv(\chi_{u-a}\nabla a + \chi_{u-b}\nabla b)\Big), \tag{16b}$$

$$\frac{\partial a}{\partial t} = \nabla^2 a + u - a, \tag{16c}$$

$$\frac{\partial b}{\partial t} = D_c\nabla^2 b + v - \delta b. \tag{16d}$$

In the above, we denote by $\chi_{u\text{-}a}$ the chemotactic sensitivity of u to signal a (and so on). In the equation for u, the terms in (1u) describe the random component to movement, terms in (2u) describe chemotactic movement of u up gradients in a and b and terms in (3u) arise from the displacement of u due to chemotaxis of v to a and b. The v equation can be interpreted analogously. With the focus on differential-chemotaxis induced patterning, we set $D = 0.01$ and assume a and b have equivalent diffusion and degradation rates ($D_c = \delta = 1$). These restrictions allow us to concentrate on those parameters defining the self- and cross-chemotactic responses, defined in Table 2.

The above equations are studied both on a 1D domain $[0, L]$ and 2D square $[0, L] \times [0, L]$ with periodic boundary conditions. We consider the same initial tissue as for the single signal case, i.e., an initial uniform total cell density $w(x, 0) = w_0$ consisting of equal proportions of the two uniformly distributed subpopulations. With these initial conditions, Eqs. (16) (with $\delta = 1$) possess a steady state at $(w_0/2, w_0/2, w_0/2, w_0/2)$; stability analysis can be performed, yet the fourth-order polynomial precludes calculation of an explicit condition for instability.

Table 2 Parameters and definitions for the self- and cross-chemotactic sensitivity parameters

	Definition	Interpretation
χ_{u-a}	self-tactic sensitivity of u	chemotactic response of u to the chemical produced by u
χ_{v-b}	self-tactic sensitivity of v	chemotactic response of v to the chemical produced by v
χ_{u-b}	cross-tactic sensitivity of u	chemotactic response of u to the chemical produced by v
χ_{v-a}	cross-tactic sensitivity of v	chemotactic response of v to the chemical produced by u

Numerical simulations were conducted as for the single signal case under variation of the 4 chemotactic sensitivities restricted to the ranges

$$-2 < \chi_{u-a}, \chi_{u-b}, \chi_{v-a}, \chi_{v-b} < 2.$$

Despite the restrictions already imposed, the taxing nature of numerics excludes complete investigation into this parameter space. Two methods were utilized: (1) chemotactic-sensitivity values were chosen randomly (within the above ranges) and (2) a systematic exploration of the "self-tactic" parameter space was conducted at specific cross-tactic sensitivity pairings. Together, this provides reasonable insight into the scope of patterning, yet it is impossible to rule out whether other behavior is possible in uncharted regions. As for the single signal case, a variety of both stationary and temporal patterns was observed.

5.2.1. Pattern types

As before, parameter regimes were found in which solutions evolved to each of the 4 main stationary pattern types described for the single signal model. An additional stationary pattern class, termed *partial engulfment* (corresponding to the terminology used to describe adhesion-driven sorting) was also found. Intuitively, this occurs when the two cell populations have strong and positive self-taxis (resulting in aggregation in response to their own signal) and a lower level of positive cross-taxis (allowing the aggregations to join together). Representatives of each of the stationary pattern types (in both 1D and 2D) are plotted in Fig. 9(i).

For a single-signal, sustained temporal behavior was found only in restricted regions of the parameter space and their formation was sensitive to factors such as domain size and initial conditions. In the extension to dual-signals, spatio-temporal patterns were both frequently observed and robust, indicating expansion to wide regions of parameter space. An expanded range of spatio-temporal patterns was identified, including analogues of some of the stationary pattern types: In Fig. 9(ii) "engulfed" and "partially-engulfed" traveling aggregations are illustrated. In 2D, these temporal patterns take the form of a migrating and patterned "slug": an aggregation develops that migrates across the domain with constant speed and within which the two subpopulations are compartmentalized. An example is shown in the bottom row of Fig. 9(ii) and a movie of this process is available at http://www.ma.hw.ac.uk/~painter/diffchemotaxis/index.html. Note that the slug simulations in 2D have employed biased initial conditions to speed up the formation of the pattern, though the same behavior is also observed using random initial data.

5.2.2. Patterning in (χ_{u-a}, χ_{v-b}) space

To determine the correspondence between sensitivity parameters and pattern type, an exploration of the self-tactic space (χ_{u-a}, χ_{v-b}) was conducted for various cross-tactic sensitivity (χ_{u-b}, χ_{v-a}) pairings. The results of the analysis are presented in the plots of

(i) Two–signal model: stationary patterns
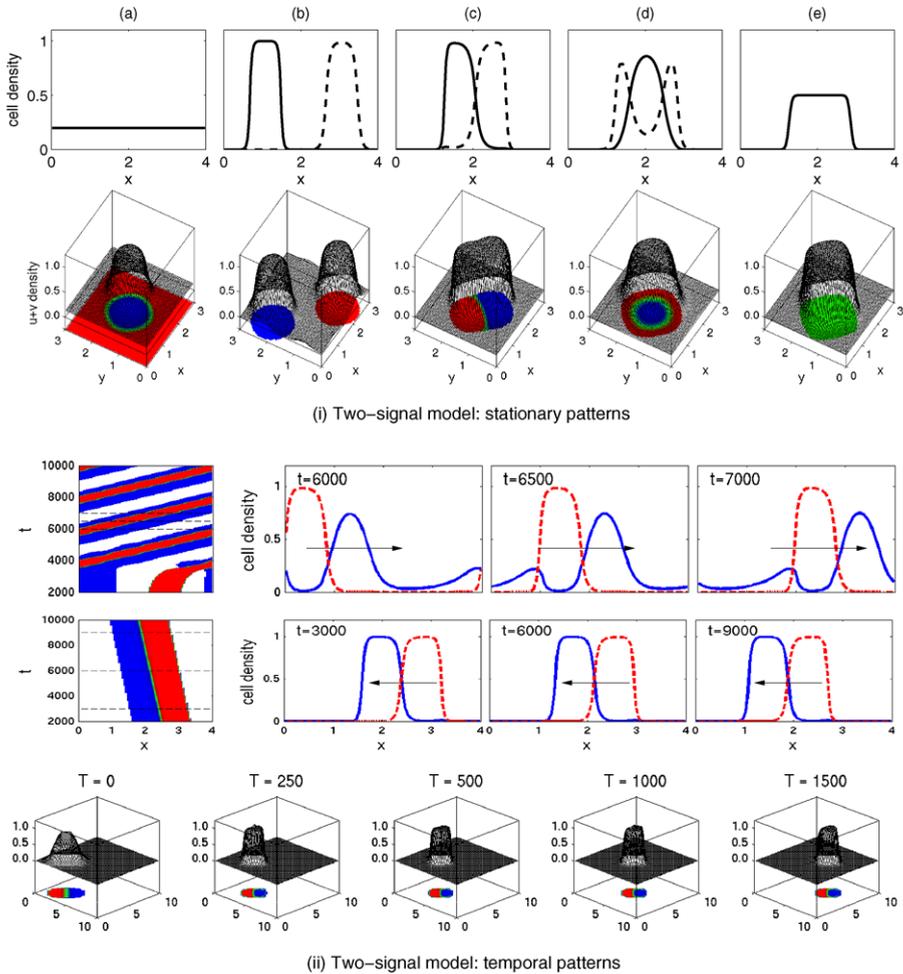

(ii) Two–signal model: temporal patterns

Fig. 9 (i) *Representative stationary patterns in the dual signal sorting model.* Distributions for u (solid line) and v (dashed line) are plotted for 1D (top row) and 2D domains at different points in $(\chi_{u-a}, \chi_{v-b}, \chi_{u-b}, \chi_{v-a})$ space. (a) Single population aggregates for $(\chi_{u-a}, \chi_{v-b}, \chi_{u-b}, \chi_{v-a}) = (2, 0, 0, 0)$, (b) Complete sorting for $(2, 1, 0, 0)$, (c) Partial engulfment for $(2, 1.5, 1.0, 0.75)$, (d) Engulfment for $(2, 0.5, 1, 1)$ and (e) Mixing for $(1, 1, 1, 1)$. In (e) the distributions of u and v are indistinguishable. Simulations as described in the Appendix on the 1D domain $[0, 4]$ (with $\Delta x = 0.05$) or 2D square $[0, 3] \times [0, 3]$ (with $\Delta x = \Delta y = 0.05$) and periodic boundary conditions. (ii) *Representative temporal patterns in the dual signal sorting model.* The first two rows demonstrate 1D temporal patterns, including an "engulfed wave" found at $(\chi_{u-a}, \chi_{v-b}, \chi_{u-b}, \chi_{v-a}) = (2, 0.5, 0, 1)$ and a "sorted wave" at $(2, 2, 0, 1)$. The left-most frame provides the space-time evolution for u (solid) and v (dashed) with successive panels to the right giving snapshots of u and v at the times indicated by dashed-lines in the space-time plot. The direction of wave propagation is indicated by the arrows. The bottom-most row shows a migrating "slug" in 2D for $(\chi_{u-a}, \chi_{v-b}, \chi_{u-b}, \chi_{v-a}) = (2, 0.5, 0, 1)$. Left to right plots show total tissue density (black mesh) and the distribution of u and v (underlying colorplot) at the times indicated. For the temporal patterns, simulations were performed as described in the numerics on the 1D domain $[0, 4]$ (with $\Delta x = 0.05$) or 2D square $[0, 10] \times [0, 10]$ (with $\Delta x = \Delta y = 0.2$) and periodic boundary conditions.
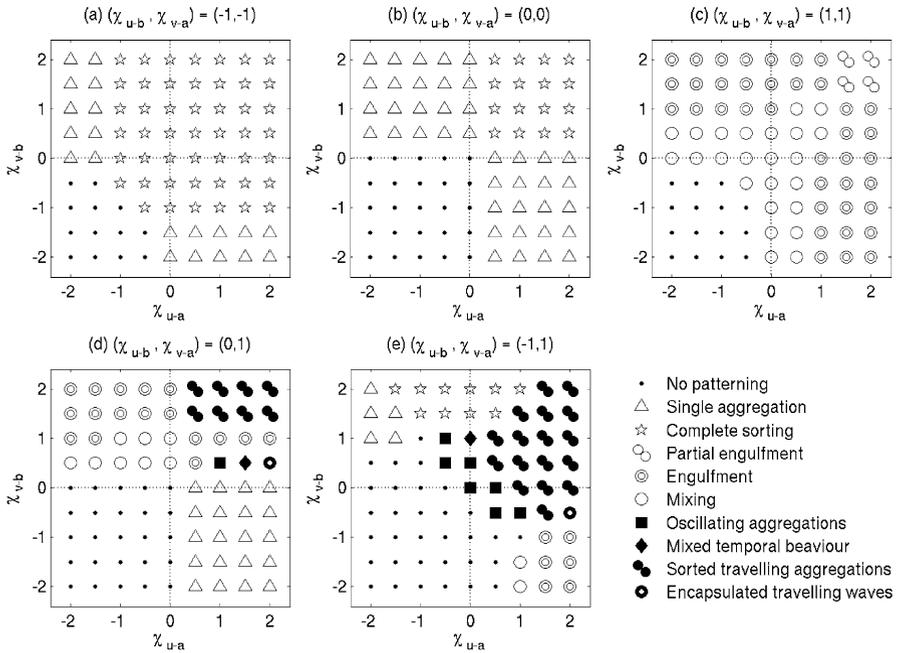
Fig. 10 Dependency between patterning form and chemotactic sensitivity values. Plots indicate the pattern type found at different points in the self-tactic sensitivity (χ_{u-a}, χ_{v-b}) space at specific cross-tactic sensitivity pairs. Patterns were classified following simulations of Eqs. (16) on a 1D domain [0, 4] (using $\Delta x = 0.08$ and periodic boundary conditions) as described in the Appendix.

Fig. 10. For symmetric cross-taxis ($\chi_{u-b} = \chi_{v-a}$, Figs. 10(a)–(c)), only stationary patterns are observed and the patterning type is symmetric in (χ_{u-a}, χ_{v-b}) space. It is worth noting that when self-tactic and cross-tactic sensitivities are all positive and $\chi_{u-b} = \chi_{v-a}$, we obtain the same pattern types at the same sensitivity relationships as determined for differential-adhesion (see Fig. 1).

For asymmetric cross-tactic responses ($\chi_{u-b} \neq \chi_{v-a}$, Figs. 10(d)–(e)), both stationary and temporal patterning can be observed. Increasing the asymmetry between the cross-tactic responses expands the region under which spatio-temporal patterning is found: the predominant spatio-temporal patterns correspond to partially-engulfed traveling aggregations as illustrated in Fig. 9(ii). Intuitively, these traveling patterns occur through sub-populations first accumulating into distinct aggregations via their self-tactic responses. An attractive cross-tactic response joins the two aggregations, yet asymmetry leads to a directional bias and ongoing movement.

6. Conclusions

In this paper, a continuous model was developed to describe movement of a tissue composed of multiple chemotactic subpopulations. By allowing cells both to migrate into free space (corresponding to a cell crawling across a substrate or through extracellular matrix)

and to migrate through displacement of neighbors (corresponding to pulling itself across the surface of another cell in a crowded tissue), the model can describe migration in both dispersed and aggregated tissues.

Application of the model to cell sorting permitted insight into the capacity for differential-chemotaxis to pattern a heterogeneous tissue: In addition to capturing the same patterns observed through differential-adhesion, the possibility of positive and negative responses and asymmetries in the cross responses expanded the range of patterning. In particular, we observed the formation of migrating and patterned "slugs" (so-called due to their qualitative likeness to those observed in *Dictyostelium*). The propulsion of these aggregations is "internally-generated"—it arises through the responses of the cells to signal gradients generated inside the mound, rather than to an external gradient.

An important point to stress is that although the model does not *explicitly* incorporate cell-adhesion, it is *implicitly* assumed: the different movement types (i.e., into free space/within tissues) require adhesion complexes to form either between cells or between cells and the extracellular substrate (e.g., ECM). Without these complexes, cells are unable to generate the forces to pull themselves past other cells or move across a surface. Here, these are phenomenologically represented in the "capacity for movement" parameters in Eqs. (5): a high value of k_i could correspond to a cell that rapidly migrates through an extracellular matrix or across an external substrate (through rapid formation/turnover of the adhesion complexes). An area for future study would be to investigate how the two processes of differential chemotaxis and adhesion may interact and enhance patterning. Intuitively, chemotaxis could allow the longer range communication between the different cell subpopulations, thereby accelerating the initial organization and sorting of the two populations. Differential adhesion may act to locally refine and modify the precise arrangements of the cell types. To address these questions in detail, however, it may be necessary to adopt a more sophisticated approach to modeling adhesion, for example, the integro-PDE based approach developed in Armstrong et al. (2006). On this note, it is tempting to speculate whether the framework can be directly extended to model adhesion: cell adhesion results from the binding of transmembrane receptors and one approach would be to replace the existing variables for diffusible extracellular chemoattractants with nondiffusing variables for the adhesive receptor concentrations. Any such approach, however, would require the receptor distributions to be correctly transported along with cell migration.

In the modeling here, a generic approach was adopted: the principal aims were to test the capacity of the model to describe the different types of migration and investigate differential-chemotaxis patterning. Therefore, simple (linear) forms were adopted to describe cell-signal interactions, however, in specific applications greater attention should be paid to the appropriate kinetics. A number of systems invite future expansion of the modeling, such as patterning in the slime mold *Dictyostelium*. As described previously, cells aggregate into a mound which undergoes differentiation into prestalk and prespore cells. The factor DIF is known to play a crucial role in the initiation, regulation and proportioning of the prespore (approximately 75%) and prestalk cells (for a review, see Kimmel and Firtel, 2004). Compartmentalization of the subpopulations is followed by the transformation to a migrating slug in which prestalk cells undergo further differentiation and organization. The distinct motility responses of prespore/prestalk cells (Early et al., 1995) has led to the hypothesis that differential-chemotaxis may pattern

Dictyostelium: Feit et al. (2007) have demonstrated that prespore cells have lower chemotactic sensitivities to prestalk cells. The modeling here supports previous theoretical studies (e.g., Pate and Othmer, 1986; Vasiev and Weijer, 1999; Palsson and Othmer, 2000; Umeda and Inouye, 2004) suggesting that differential chemotaxis may play a role in *Dictyostelium* patterning. Clearly, the continuous framework presents a convenient approach to expand the analysis such that the various factors (e.g., cell subpopulations, cAMP, DIF, *etc.*) can be integrated and their contribution to the patterning process understood.

A second area for future modeling is control of cell movement during early embryonic development: chick gastrulation is coordinated through the primitive streak, a transitory structure that extends anteriorly across the developing embryo from the posterior pole before retreating posteriorly and laying down the neural tube and notochord in its wake. Studies by Yang et al. (2002) reveal that cells undergo complex and coordinated migration pathways during gastrulation and that a combination of chemoattractants and chemorepellants direct primitive streak cells. The capacity of the model to incorporate multiple motile cell populations offers a method to investigate competing theories as to how these processes are coordinated.

A number of mathematical questions also arise from the modeling. During the derivation of the equations, it was assumed that cells could either move into free space (if available) or displace neighbors when confronted by a packed tissue. Clearly, it is reasonable to expect solutions should remain bounded between zero and the maximum tissue density. The numerical simulations presented earlier indicate that this is the case: in none of the cases considered were the densities for u, v or $u + v$ observed to decrease below zero or increase above 1. A rigorous demonstration of this in Eqs. (6) remains unaddressed. It is worth noting, however, that the limiting "crowded tissue" model (11) is identical to the volume-filling model of Hillen and Painter (2001); here, boundedness is known and, furthermore, solutions exist globally in time.

A second question arises from the study into sorting: the numerical approach adopted here illustrates the patterning range and indicates the coincidence between pattern type and parameter values. The derivation of a more explicit relationship, however, will require more detailed analysis. A further question lies in the form and speed of temporal patterns: as seen in Fig. 9(ii), traveling wave aggregations develop with distinct wavespeeds. Observations alone suggest that the speed of these waves depends on the magnitude of the chemotactic sensitivities and, in particular, the degree of asymmetry in the cross-tactic responses. Determining a more precise dependency of the wavespeed on model parameters remains to be explored.

The mechanisms underpinning the patterning of the embryo remain one of the outstanding questions in biology. The capacity for certain cell types to migrate in response to environmental signals is crucial not only to embryonic patterning, but also in physiological and pathological processes of the adult: e.g., cell migration during tumor invasion is believed to be a key step in the formation of metastases. While we have focused on a simple two-population system here, the continuous framework developed offers a flexible approach through which a wide range of complex biological processes can be modeled.

Appendix A: Details of the numerical scheme

The numerical simulations employ a Method of Lines approach to solve the generic Eqs. (6) in which spatial terms are initially discretized to yield a system of time-dependent ODEs (the MOL-ODEs). Spatial terms comprise of diffusive and advective terms for cell movement and are approximated in conservative form. For the discretization, the 1D (2D) domain is uniformly discretized into n_x ($n_x \times n_y$) points of spacing Δx (Δx, Δy). We note that the spatial discretization varied in different simulations to ensure reasonably accuracy while minimizing computational cost. For the advective terms, we employed a first order upwinding scheme while the diffusive terms are solved using a standard central difference scheme: possible extensions for a future investigation would be to consider higher order upwinding schemes to limit the impact from numerical diffusion. Integration in time of the MOL-ODE systems was performed using an implicit scheme (and compared with an explicit scheme for testing): here we employed the ROWMAP stiff systems integrator (Weiner et al., 1997, see also Gerisch and Chaplain, 2007 for its application in other models of cell movement). A detailed investigation into the relative advantages of different time schemes for optimal balance between accuracy and computational cost would be necessary for future applications.

In the numerical investigations, equations were solved until either a maximum time limit was reached (arbitrarily set at $t = 10000$) or until solutions had converged to a numerically-defined steady state. On a 1D domain $[0, L]$ we calculated

$$\frac{1}{T} \frac{1}{L} \sum_{i=1}^{n_x} \Delta x \left| \left(c_j(x_i, t + T) - c_j(x_i, t) \right) \right|$$

for each species c_j, where $c_j(x_i, t)$ represents the numerical approximation at position x_i and time t. Solutions were stopped if

$$\max(c_j, j = 1 \ldots n_s) < C_{SS},$$

where n_s is the number of species. For the simulations here, we used $C_{SS} = 10^{-6}$ and $T = 25.0$. Simulations were also performed with smaller C_{SS}, however, the time taken for solutions to converge is extended. Note that it is impossible to rule out whether the solutions obtained represented the true steady state solution or a long-time transient.

Appendix B: Derivation of the two signal model

We assume the discrete-space, continuum time model given by Eqs. (3). Assuming cells migrate in response to two chemotactic signals (a and b), we take

$$P_x^{1\pm} = k_u^1 \left(1 + \kappa_{u-a}(a_{x \pm h} - a_x) + \kappa_{u-b}(b_{x \pm h} - b_x) \right),$$

$$P_x^{3\pm} = k_u^3 \big(1 + \kappa_{u-a}(a_{x\pm h} - a_x) + \kappa_{u-b}(b_{x\pm h} - b_x)\big),$$

$$Q_x^{1\pm} = k_v^1 \big(1 + \kappa_{v-a}(a_{x\pm h} - a_x) + \kappa_{v-b}(b_{x\pm h} - b_x)\big),$$

$$Q_x^{3\pm} = k_v^3 \big(1 + \kappa_{v-a}(a_{x\pm h} - a_x) + \kappa_{v-b}(b_{x\pm h} - b_x)\big).$$

We substitute the above into Eqs. (3), derive the continuum limit and extend to 2D as before. Assuming linear signal kinetics in which a is only produced by u and b is only produced by v,

$$\frac{\partial u}{\partial t} = \alpha_u \nabla\big((1-w)\nabla u + u\nabla w\big) + (\beta_u + \beta_v)\nabla(v\nabla u - u\nabla v)$$

$$- \alpha_u \phi_{u-a}\nabla\big((1-w)u\nabla a\big) - (\beta_u\phi_{u-a} - \beta_v\phi_{v-a})\nabla(uv\nabla a)$$

$$- \alpha_u \phi_{u-b}\nabla\big((1-w)u\nabla b\big) - (\beta_u\phi_{u-b} - \beta_v\phi_{v-b})\nabla(uv\nabla b),$$

$$\frac{\partial v}{\partial t} = \alpha_v \nabla\big((1-w)\nabla v + v\nabla w\big) + (\beta_v + \beta_u)\nabla(u\nabla v - v\nabla u)$$

$$- \alpha_v \phi_{v-a}\nabla\big((1-w)v\nabla a\big) - (\beta_v\phi_{v-a} - \beta_u\phi_{u-a})\nabla(uv\nabla a)$$

$$- \alpha_v \phi_{v-b}\nabla\big((1-w)v\nabla b\big) - (\beta_v\phi_{v-b} - \beta_u\phi_{u-b})\nabla(uv\nabla b),$$

$$\frac{\partial a}{\partial t} = D_a \nabla^2 a + \mu u - \delta_a a,$$

$$\frac{\partial b}{\partial t} = D_b \nabla^2 b + \nu v - \delta_b b,$$

where

$$\alpha_{u,v} = \lim_{\lambda\to\infty, h\to 0} k_{u,v}^1 \lambda h^2,$$

$$\beta_{u,v} = \lim_{\lambda\to\infty, h\to 0} k_{u,v}^3 \lambda h^2,$$

$$\phi_{u-a,u-b,v-a,v-b} = \lim_{\lambda\to\infty, h\to 0} 2\kappa_{u-a,u-b,v-a,v-b} \lambda h^2.$$

The above can be interpreted analogously to Eqs. (6): the additional terms in the cell dynamics stem from the response to the additional chemotactic signal. Assuming (13) in the above and introducing the nondimensional scalings,

$$\hat{t} = \delta_a t, \qquad \hat{\mathbf{x}} = \sqrt{\frac{D_a}{\delta_a}}\mathbf{x}, \qquad \hat{a} = \frac{\delta_a}{\mu}a, \qquad \hat{b} = \frac{\delta_a}{\nu}b, \qquad D = \frac{\alpha}{D_a}, \qquad D_c = \frac{D_b}{D_a},$$

$$\chi_{u-a} = \frac{\phi_{u-a}\mu}{D_a\delta_a}, \qquad \chi_{u-b} = \frac{\alpha\phi_{u-b}\mu}{D_a\delta_a}, \qquad \chi_{v-a} = \frac{\alpha\phi_{v-a}\nu}{D_a\delta_a}, \qquad \chi_{v-b} = \frac{\alpha\phi_{v-b}\nu}{D_a\delta_a}.$$

we arrive (after dropping the "hats") at Eqs. (16).

References

Alt, W., 1980. Biased random walk model for chemotaxis and related diffusion approximation. J. Math. Biol. 9, 147–177.

Armstrong, N.J., Painter, K.J., Sherratt, J.A., 2006. A continuum approach to modelling cell-cell adhesion. J. Theor. Biol. 243, 98–113.

Byrne, H., Owen, M., 2004. A new interpretation of the Keller–Segel model based on multiphase modelling. J. Math. Biol. 49, 604–626.

Charron, F., Tessier-Lavigne, M., 2005. Novel brain wiring functions for classical morphogens: a role as graded positional cues in axon guidance. Development 132, 2251–2262.

Condeelis, J., Singer, R., Segall, J., 2005. The great escape: when cancer cells hijack the genes for chemotaxis and motility. Annu. Rev. Cell Dev. Biol. 21, 695–718.

Dallon, J., Othmer, H., 2004. How cellular movement determines the collective force generated by the *Dictyostelium discoideum* slug. J. Theor. Biol. 231, 203–222.

Dormann, D., Weijer, C., 2006. Chemotactic cell movement during *Dictyostelium* development and gastrulation. Curr. Opin. Genet. Dev. 16, 367–373.

Early, A., Abe, T., Williams, J., 1995. Evidence for positional differentiation of prestalk cells and for a morphogenetic gradient in *Dictyostelium*. Cell 83, 91–99.

Feit, I., Pawlikowski, J., Zawilski, C., 2007. A model for cell type localization in the migrating slug of *Dictyostelium discoideum* based on differential chemotactic sensitivity to cAMP and differential sensitivity to suppression of chemotaxis by ammonia. J. Biosci. 32, 329–338.

Foty, R.A., Steinberg, M.S., 2004. Cadherin-mediated cell-cell adhesion and tissue segregation in relation to malignancy. Int. J. Dev. Biol. 48, 397–409.

Friedl, P., Brocker, E.B., 2000. The biology of cell locomotion within three-dimensional extracellular matrix. Cell Mol. Life Sci. 57, 41–64.

Gatenby, R., Gawlinski, E., 1996. A reaction–diffusion model of cancer invasion. Cancer Res. 56, 5745–5753.

Gerisch, A., Chaplain, M., 2007. Mathematical modelling of cancer cell invasion of tissue: local and non-local models and the effect of adhesion. J. Theor. Biol. 250, 684–704.

Glazier, J.A., Graner, F., 1993. Simulation of the differential adhesion driven rearrangement of biological cells. Phys. Rev. E 47(3), 2128–2154.

Heldin, C.-H., Westermark., B., 1999. Mechanism of action and in vivo role of platelet-derived growth factor. Physiol. Rev. 79, 1283–1316.

Hillen, T., 2002. Hyperbolic models for chemosensitive movement. Math. Models Methods Appl. Sci. 12(7), 1007–1034.

Hillen, T., Painter, K., 2001. A parabolic model with bounded chemotaxis—prevention of overcrowding. Adv. Appl. Math. 26, 280–301.

Hillen, T., Painter, K.J., 2009. A user's guide to PDE models for chemotaxis. J. Math. Biol. 58, 183–217.

Höfer, T., Sherratt, J., Maini, P., 1995. Dictyostelium discoideum: cellular self-organisation in an excitable biological medium. Proc. R. Soc. Lond. B 259, 249–257.

Keller, E., Segel, L., 1970. Initiation of slime mold aggregation viewed as an instability. J. Theor. Biol. 26, 399–415.

Keller, E., Segel, L., 1971. Model for chemotaxis. J. Theor. Biol. 30, 225–234.

Kimmel, A., Firtel, R., 2004. Breaking symmetries: regulation of *Dictyostelium* development through chemoattractant and morphogen signal-response. Curr. Opin. Genet. Dev. 14, 540–549.

Larrivee, B., Karsan, A., 2000. Signaling pathways induced by vascular endothelial growth factor (review). Int. J. Mol. Med. 5, 447–456.

Lauffenburger, D., Horwitz, A., 1996. Cell migration: a physically integrated molecular process. Cell 84, 359–369.

Luca, M., Chavez-Ross, A., Edelstein-Keshet, L., Mogilner, A., 2003. Chemotactic signaling, microglia, and Alzheimer's disease senile plaques: is there a connection?. Bull. Math. Biol. 65, 693–730.

Matsukuma, S., Durston, A., 1979. Chemotactic cell sorting in *Dictyostelium discoideum*. J. Embryol. Exp. Morphol. 50, 243–251.

Montell, D., 2006. The social lives of migrating cells in *Drosophila*. Curr. Opin. Genet. Dev. 16, 374–383.

Murdoch, C., Giannoudis, A., Lewis, C., 2004. Mechanisms regulating the recruitment of macrophages into hypoxic areas of tumors and other ischemic tissues. Blood 104, 2224–2234.

Murray, J., 2003. On the mechanochemical theory of biological pattern formation with application to vasculogenesis. C.R. Biol. 326, 239–252.

Nardi, J., 1994. Rearrangement of epithelial cell types in an insect wing monolayer is accompanied by differential expression of a cell surface protein. Dev. Dyn. 199, 315–325.

Odell, G., Bonner, J.T., 1986. How the *Dictyostelium discoideum* grex crawls. Philos. Trans. R. Soc. Lond. 312, 487–525.

Othmer, H., Stevens, A., 1997. Aggregation, blowup and collapse: the ABC's of generalized taxis. SIAM J. Appl. Math. 57, 1044–1081.

Othmer, H., Dunbar, S., Alt, W., 1988. Models of dispersal in biological systems. J. Math. Biol. 26, 263–298.

Painter, K., Sherratt, J.A., 2003. Modelling the movement of interacting cell populations. J. Theor. Biol. 225, 325–337.

Painter, K., Maini, P., Othmer, H., 2000. Development and applications of a model for cellular response to multiple chemotactic cues. J. Math. Biol. 41, 285–314.

Painter, K.J., Hillen, T., 2002. Volume-filling and quorum-sensing in models for chemosensitive movement. Can. Appl. Math. Q. 10, 501–544.

Palsson, E., Othmer, H., 2000. A model for individual and collective cell movement in *Dictyostelium discoideum*. Proc. Natl. Acad. Sci. USA 97, 10448–10453.

Pate, E., Othmer, H., 1986. Differentiation, cell sorting and proportion regulation in the slug stage of *Dictyostelium discoideum*. J. Theor. Biol. 118(3), 301–319.

Patlak, C., 1953. Random walk with persistence and external bias. Bull. Math. Biophys. 15, 311–338.

Sherratt, J.A., 2000. Wavefront propagation in a competition equation with a new motility term modelling contact inhibition between cell populations. Proc. R. Soc. Lond. A 456, 2365–2386.

Sherratt, J.A., Nowak, M.A., 1992. Oncogenes, anti-oncogenes and the immune response to cancer. Proc. R. Soc. Lond. B 248, 261–272.

Simpson, M.J., Landman, K.A., Hughes, B.D., Newgreen, D., 2006. Looking inside an invasion wave of cells using continuum models: proliferation is the key. J. Theor. Biol. 243, 343–360.

Steinberg, M.S., 2007. Differential adhesion in morphogenesis: a modern view. Curr. Opin. Gen. Dev. 17, 281–286.

Townes, P., Holtfreter, J., 1955. Directed movements and selective adhesion of embryonic amphibian cells. J. Exp. Zool. 128, 53–120.

Turing, A.M., 1952. The chemical basis of morphogenesis. Philos. Trans. R. Soc. Lond. B 237, 37–72.

Tyson, R., Lubkin, S., Murray, J., 1999. Model and analysis of chemotactic bacterial patterns in a liquid medium. J. Math. Biol. 38, 359–375.

Umeda, T., 1993. A thermodynamical model of cell distributions in the slug of cellular slime mold. Bull. Math. Biol. 55, 451–464.

Umeda, T., Inouye, K., 1999. Theoretical model for morphogenesis and cell sorting in *Dictyosteilium discoideum*. Physica D 126, 189–200.

Umeda, T., Inouye, K., 2004. Cell sorting by differential cell motility: A model for pattern formation in *Dictyostelium*. J. Theor. Biol. 226, 215–224.

Vasiev, B., Weijer, C., 1999. Modeling chemotactic cell sorting during *Dictyostelium discoideum* mound formation. Biophys. J. 76, 595–605.

Webb, S., Owen, M., Byrne, H., Murdoch, C., Lewis, C., 2007. Macrophage-based anti-cancer therapy: modelling different modes of tumour targeting. Bull. Math. Biol. 69, 1747–1776.

Weiner, R., Schmitt, B., Podhaisky, H., 1997. Rowmap—a row-code with Krylov techniques for large stiff odes. Appl. Numer. Math. 25, 303–319.

Wolpert, L., 1969. Positional information and the spatial pattern of cellular differentiation. J. Theor. Biol. 25, 1–47.

Woodward, D., Tyson, R., Myerscough, M., Murray, J., Budrene, E., Berg, H., 1995. Spatiotemporal patterns generated by *Salmonella-typhimurium*. Biophys. J. 68(5), 2181–2189.

Wu, D., 2005. Signaling mechanisms for regulation of chemotaxis. Cell Res. 15, 52–56.

Yang, X., Dormann, D., Münsterberg, A., Weijer, C., 2002. Cell movement patterns during gastrulation in the chick are controlled by positive and negative chemotaxis mediated by FGF4 and FGF8. Dev. Cell 3, 425–437.

Yue, Q., Wagstaff, L., Yang, X., Weijer, C., Münsterberg, A., 2008. Wnt3a-mediated chemorepulsion controls movement patterns of cardiac progenitors and requires RhoA function. Development 135, 1029–1037.